Title
Characterization of spray atomization of 3003 aluminum alloy during linear spray atomization and deposition

Journal
Metallurgical and Materials Transactions B, 29(4)

ISSN
1073-5615

Authors
Zhou, Yizhang
Lee, Steven
McDonell, Vincent G
et al.

Publication Date
1998-08-01

DOI
10.1007/s11663-998-0138-3

Characterization of Spray Atomization of 3003 Aluminum Alloy during Linear Spray Atomization and Deposition

YIZHANG ZHOU, STEVEN LEE, VINCENT G. McDONELL, SCOTT SAMUELSEN, ROBERT L. KOZAREK, and ENRIQUE J. LAVERNIA

Linear spray atomization and deposition is an attractive technique to produce near-net-shape deposits, such as aluminum sheet and strip. In the present study, phase Doppler interferometry (PDI) was used in a backscatter mode to characterize, *in situ*, the droplet size and velocity distributions during linear spray atomization and deposition of a 3003 aluminum alloy. The PDI measurements were obtained along axes corresponding to the direction parallel to the nozzle slit and to the direction perpendicular to the slit. The PDI results delineate the temporal and spatial distribution of the droplet size and velocity during the metal spray. Both point and ''line'' measurements were obtained and are reported. The line measurements resulted from the integration of measurement made along a line scan obtained in real time (*i.e.*, not ensemble averaged). Postrun analysis of the droplet size distribution using laser diffraction and sieving techniques is also reported. The PDI point measurements revealed that droplet size and velocity distribution were relatively invariant with time. The line measurements of droplet velocity showed that the droplet axial velocity exhibits a bimodal behavior, which becomes more apparent with increasing atomizing gas pressure, a result of droplet recirculation inside the spray chamber. In addition, the peak in the droplet axial velocity distribution increased as atomizing gas pressure increased. The line characterization also showed that the droplet size distribution became more homogeneous with increasing gas pressure, and that the distribution characteristic diameters of droplets decreased consistently with increasing gas pressure. Postrun characterization of the droplet size distribution of the entire metal spray using diffraction and sieving methods indicated that the mass (volume) median diameter D_{50} and the Sauter mean diameter (SMD) D_{32} decreased with increasing gas pressure in a manner consistent with PDI results.

I. INTRODUCTION

SPRAY atomization by an inert gas is a fundamental step in spray forming, a manufacturing technique in which metal droplets are sprayed onto a substrate to produce a fine-grained, microstructurally homogeneous material.[1,2,3] In order to produce near-net-shape deposited materials, investigators are exploring methods to control the spatial distribution of droplets in the spray. For example, experimental results indicate that, for metal sprays produced by circular atomizers, the droplet mass distribution exhibits either (1) a Gaussian distribution centered about the spray axis[4–7] or (2) a bimodal distribution.[8,9] The deposit shape resembles the spatial distribution of droplet mass arriving at the deposition surface.[5,7,10] To circumvent this apparent limitation, a variety of novel experimental arrangements have been developed, and it is now possible to spray form a variety of geometries, including rings,[11,12] billets,[12,13,14] tubes,[12,15–17] and cylinders.[12] More recently, however, the application of spray forming technology using a linear atomizer arrangement, also defined as linear spray atomization and deposition, has attracted considerable interest for the continuous production of Al sheet and strip as a result of economic incentives, such as reduced energy requirements, reduced costs, and improved mechanical properties compared to conventional ingot casting and hot-rolling process.[18,19] Figure 1 illustrates an approach for linear spray atomization and deposition. Potential benefits derived from the atomization of metals using a linear spray deposition approach are as follows:

1. improved droplet spatial distribution;
2. high productivity;
3. high aspect ratio (i.e., wide sheets can be produced); and
4. low overspray yields.

Droplet size and spatial distribution in the spray will also significantly affect (1) the solidification behavior of individual droplets, (2) the solidification behavior of the spray-deposited materials, and (3) the porosity volume distribution in the spray-deposited materials. In addition to size and spatial distribution, droplet velocity is also important since it determines the droplet flight time and heat transfer characteristics. Therefore, characterization of droplet size and velocity distribution may ultimately feed back to operating variables that control a metal spray. Among the techniques used to simultaneously determine droplet velocity and size distribution, phase Doppler interferometry (PDI) is the most mature.[20] Spatially resolved, *in situ*, measurement of droplet size and velocity using PDI provides detailed information regarding the structure of a spray,[21,22,23] enabling additional insight into the mechanics of the process to be gained. Although PDI is well established for the character-

YIZHANG ZHOU, Graduate Student Researcher, Chemical and Biochemical Engineering and Materials Science Department, STEVEN LEE, Engineer, VINCENT G. McDONELL, Senior Engineer, and SCOTT SAMUELSON, Professor, Department of Mechanical and Aerospace Engineering, and ENRIQUE J. LAVERNIA, Professor and Chair, Department of Chemical and Biochemical Engineering and Materials Science and Department of Mechanical and Aerospace Engineering, are with the University of California-Irvine, Irvine, CA 92697. ROBERT L. KOZAREK, Technical Specialist, is with the Fluid State Process Design Center, Aluminum Company of America, Alcoa Center, PA 15069.

Manuscript submitted December 9, 1996.

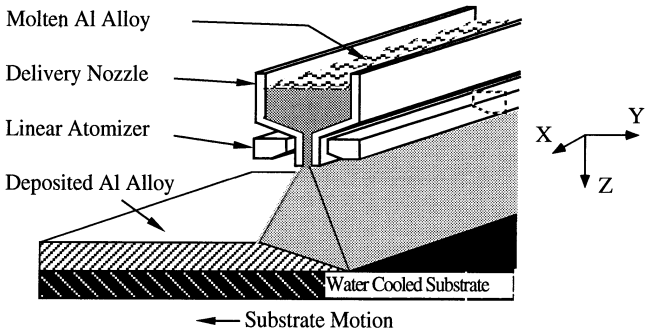

Fig. 1—Schematic of spray deposition of aluminum alloy using a linear atomizer.

ization of sprays produced by a variety of techniques,[20] it has not been widely applied to sprays of the type that are of interest in spray forming metallic materials. Inspection of the literature revealed some examples of PDI measurements of droplet velocity and size distribution, as well as gas velocity, for water sprays (typically used to simulate metal sprays) produced by the circular atomizer arrangements typically used in metal spray processes[4] and for metal sprays produced by the circular atomizer arrangements.[24–27] It has been reported[9,27] that PDI characterization of the spray behavior for circular atomizer conditions showed reasonable agreement with predicted results using one- or multidimensional mathematical models. Moreover, in the case of metal sprays, evidence also suggested that conventional signal processing methods (*e.g.*, counter processors) may not be adequate for the noisy environment encountered in metal sprays due to surface imperfections, spray density, and optical effects such as beam steering.[28,29,30] Therefore, state-of-the-art signal processing is desired for difficult environments, such as those typically associated with molten metals. In previous studies,[31] a fiber optic–based frequency domain system was applied to characterize water sprays produced by linear atomizers. Preliminary results[31] showed that frequency domain processing was less sensitive to detector gain than counter-based systems especially in backscatter operation as required for sizing opaque metal droplets.

The overall goal of the current study was to use PDI to characterize and establish the relationship of spray performance to spray-formed aluminum sheet during the linear spray atomization and deposition process. The objectives of the current effort are (1) acquisition of PDI measurements of the droplet velocity and size distribution in metal sprays produced by linear atomization; (2) analysis of the influence of process variables, such as atomizing gas pressure, on droplet velocity and size distribution; and (3) comparison of the powder droplet size distributions obtained by PDI, laser diffraction, and mechanical sieving.

II. EXPERIMENTAL PROCEDURES

The UCI linear spray forming facility used in the present experiments is comprised of a spray chamber (1060 mm in diameter and 2500 mm in height), linear atomizer unit, induction unit, dynamic substrate for deposition, gas manifold, gas exhaust, and powder collection system. For the atomization of 3003 aluminum alloys (Al-1.12Mn-0.57Si-0.69Fe-0.15Cu, wt pct), the ingot alloys were remelted and superheated using a 25-kW induction unit to a temperature of 150 °C above the equilibrium liquidus, and melts were maintained for 15 to 20 minutes to ensure uniform temperature. The weight of alloy charged for each experiment was 2.25 ± 1 pct kg. The melts were then allowed to fall through a liquid metal delivery nozzle by lifting the stopper inside the crucible and atomized into a distribution of micrometer-size droplets using nitrogen gas. For the present study, gas pressure drops from 310 to 379 kPa were considered. The corresponding gas flow rates were measured with a laminar flow element (Mariam Instrument, Cleveland, OH), and a summary of the measured gas flow rates is listed in Table I. To reduce oxidation, the experiments were conducted inside an environmental chamber, which was evacuated and backfilled with nitrogen to a pressure of 6895 Pa (1 psig) prior to melting and atomization. The primary atomization variables used in the present study are listed in Table I. A phase Doppler interferometer (Aerometrics RSA, Sunnyvale, CA) was used to characterize, *in situ*, the metal spray behavior, droplet size, and velocity simultaneously. The atomized aluminum powders were collected and sampled, and postrun analysis of droplet size and distribution of the collected powders was carried out. The droplet size distributions were determined by (1) mechanical sieving according to ASTM standard B214 and MPIF standard 5 and (2) an ensemble laser diffraction technique (*Insitec* EPCS, San Ramon, CA).

Phase Doppler interferometry is a single droplet counting technique which can, in principle, be used for on-line measurement of the atomized powder size and velocity. The technique is an extension of laser Doppler anemometry, in which two laser beams are intersected at the region of interest, forming an interferometric sampling volume. When a droplet passes through the sampling volume, it scatters the interference pattern into space. This scattered light is collected by a pair of detectors that are used to determine spatial and temporal frequency of the pattern. The spatial frequency is related to size and the temporal frequency is related to velocity. Figure 2 illustrates the facility setup (top view) used for the experimental measurements of droplet velocity and size using PDI. The Real Signal Analyzer transmitter and receiver were set with a 145 deg collection angle aligned with the optical view ports designed on the chamber. The laser beams passed through the optical view ports and were focused at the center of the liquid metal nozzle in line with the nozzle slit. A 750-mm focal lens was used with a 56.9-mm beam spacing resulting in an optically limited minimum measurable size of 4 μm. Note that the minimum size could be further reduced if the beam

Table I. Experimental Variables and Physical Properties

Atomizing air pressure differentials	310 kPa (45 psig) 345 kPa (50 psig) 379 kPa (55 psig)
Gas flow rate, m^3/s ($\times 10^{-2}$)	2.01 at 310 kPa 2.22 at 345 kPa 2.44 at 379 kPa
Slit width of liquid delivery nozzle	508 μm (0.02 in.)
Slit length of liquid delivery nozzle	50.8 mm (2.0 in.)
Slit width of linear gas atomizer	508 μm (0.02 in.)
Slit length of linear gas atomizer	50.8 mm (2.0 in.)

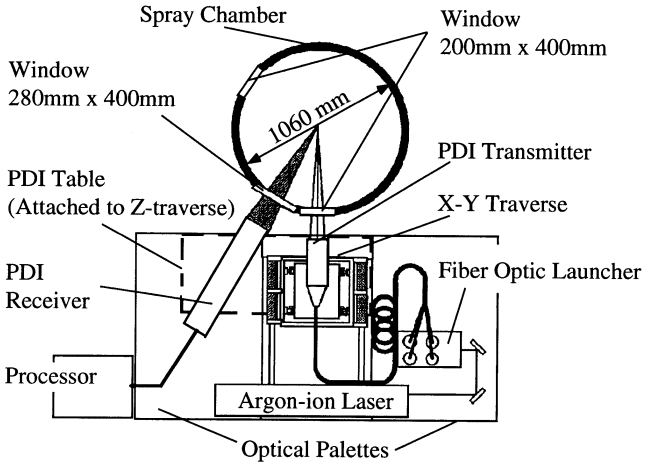

Fig. 2—Diagnostic layout on spray deposition facility.

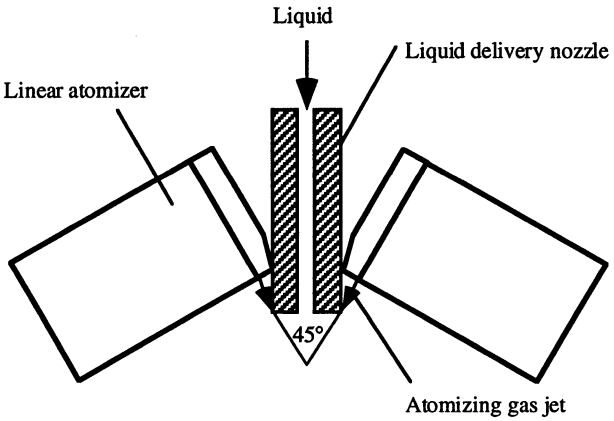

Fig. 3—Schematic of liquid delivery nozzle and a pair of linear atomizers, also showing the interaction of the atomizing gas jets with the liquid delivery nozzle.

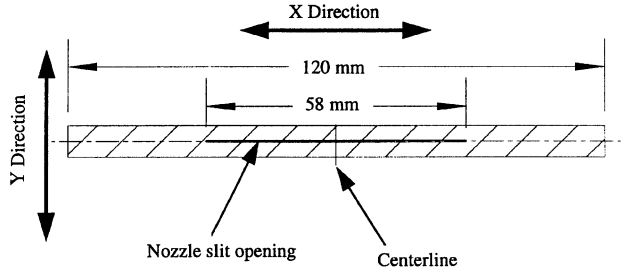

Fig. 4—Schematic of linear liquid delivery nozzle with X and Y measurement directions.

spacing were further increased or shorter focal length lenses were used. In view of the optical access limitations associated with the spray chamber, the PDI sample volume was located at an axial distance of $Z = 152.4$ mm down from the tip of the linear liquid delivery nozzle, which was the nearest distance at which measurements could be obtained for the current setup.

Since (1) PDI is inherently a point measurement and (2) each metal spray experiment run lasted only about 20 seconds, applying PDI in the conventional operating mode of one measurement point per experiment run created obvious challenges. Previous studies[32] indicated that the PDI measured Sauter mean diameter (SMD) varied in the spray plane. As a result, an alternate way of taking data was explored and an approach in which the sample volume was scanned through the spray in real time was established and implemented. During the metal spray run, the sample volume was scanned through the spray along either the X or Y direction (Figure 1) by using an X-Y motorized traverse system. The actual scanned locations, such as starting and terminating positions of measurements, were recorded by an X-Y digital readout. Due to the optical access limitations, data acquired during the experiments were from $X = +80$ mm to $X = -40$ mm along the liquid delivery nozzle slit opening direction (X traverse) and $Y = +70$ mm to $Y = -30$ mm along the direction perpendicular to the liquid nozzle slit (Y traverse).

Figure 3 shows a schematic of the linear atomizer assembly used in the present study. Although the nozzle was designed to provide flexibility in the relative angle and axial location of the atomizing gas jets to the liquid, the baseline atomizing angle was chosen as 45 deg for the present study. The dimensions of both the linear gas atomizer slit and the liquid delivery nozzle slit were 0.508×50.8 mm. The relative distance between the gas atomizer exit and the liquid nozzle tip was about 7.6 mm.

Figure 4 shows the geometry of the liquid delivery nozzle and the X, Y coordinate system (also shown in Figure 1) used for the study. The X corresponded to the direction along the slit opening, Y corresponded to the direction perpendicular to the slit opening, and Z (not shown in Figure 4) represented the vertical distance away from the exit of the liquid delivery nozzle.

III. RESULTS AND DISCUSSIONS

As discussed in the previous sections, metal powder droplet size distribution and velocity significantly influence the shape of the deposited material, solidification behavior of the droplets, and microstructural evolution of the deposited material. In the sections that follow, results of size and velocity distributions of metal powder droplets obtained by PDI and size distribution of powder droplets established by laser diffraction and sieving are presented and discussed.

Droplet size characteristics can be described in various representations. The phase Doppler particle analyzer directly measures the diameter of individual droplets, resulting in a size distribution. Various characteristic diameters such as numerical (arithmetic) mean diameter (D_{10}), ''surface mean'' diameter (D_{20}), ''volume mean'' diameter (D_{30}), and SMD (D_{32}) can then be determined. Unfortunately, some of the characteristic diameters are referred to as means, when some are, in fact, not means in the statistical sense. For example, D_{20} and D_{30} are not means based on a statistical definition but are useful characteristic diameters, as explained subsequently. The general expression for characteristic diameters was given as[33]

$$D_{pq} = \left[\sum_{i=1}^{N} D_i^p \Big/ \sum_{i=1}^{N} D_i^q \right]^{1/(p-q)} \qquad [1]$$

where N is the measured particle number. The term D_{pq} is

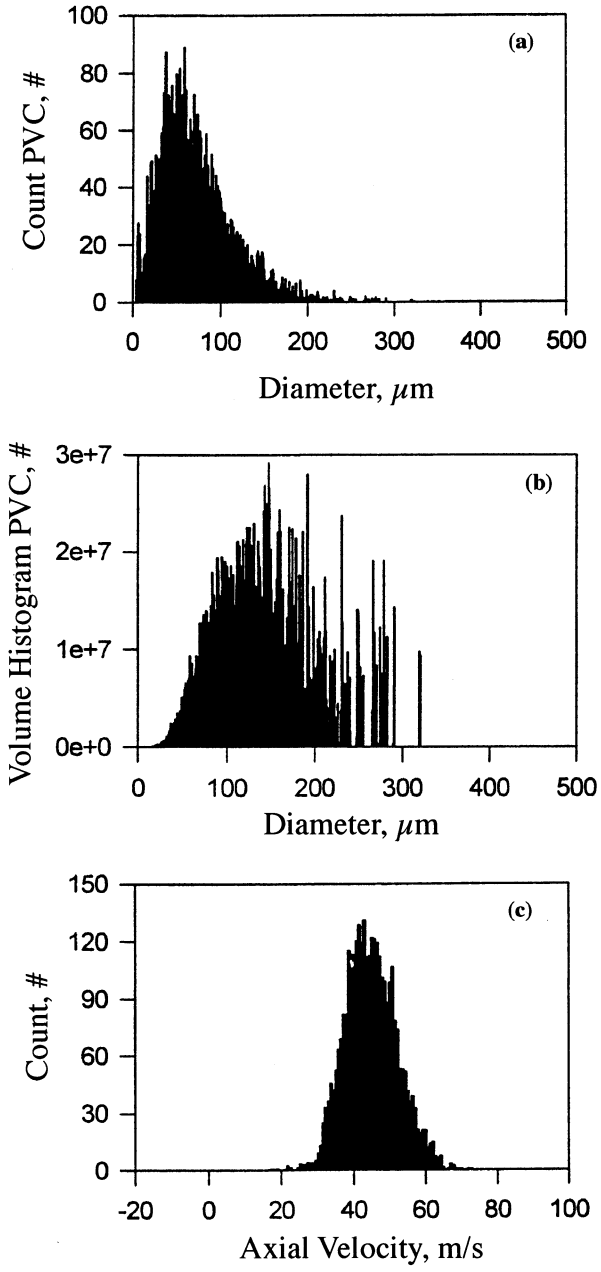

Fig. 5—Measurements at a fixed position of $X = 20$ mm, $Y = 0$, and $Z = 152.4$ mm for an atomizing gas pressure of 310 kPa (run 13): (*a*) droplet count, (*b*) droplet volume histogram, and (*c*) the axial velocity (PVC = probe volume correction).

a characteristic diameter with dissimilar orders of p and q. The distribution D_{20} represents the diameter of a droplet whose surface area times the total number of droplets, N, is equal to the total surface area of the entire spray. The distribution D_{30} represents the diameter whose volume times the number of droplets, N, is equal to the total volume of the entire spray. The SMD, D_{32}, is used to represent the size of a droplet that has the same ratio of surface area to mass (or volume) as that of the entire spray.[10] The SMD is often quoted in the characterization of metal powders, because its surface area dependency provides a useful droplet shape dependency and its volume dependency characterizes heat content of the droplet.[10]

Table II. PDI Results of D_{10}, D_{20}, D_{30}, D_{32}, Mean Velocity, and rms

	Run 13	Run 17	Run 18	Run 19	Run 20
ΔP, kPa	310	379	345	310	310
D_{10}, μm	71.55	24.3	24.42	43.6	37.17
D_{20}, μm	83.4	36.32	38.1	58.7	52.8
D_{30}, μm	94.25	51.3	55.6	74.6	69.29
D_{32}, μm	121.1	102.2	118.1	120.4	119.4
Mean V, m/s	47.1	56.4	51.5	47.3	47.3
rms, m/s	8.9	22.8	21.1	21.3	17.6

A. *Single Point Characteristics of Droplet Size and Velocity*

Figure 5 shows the results of droplet size, volume histogram, and velocity distributions obtained at a fixed measurement position of $X = 20$ mm, $Y = 0$, and $Z = 152.4$ mm for an atomizing gas pressure of 310 kPa. Figure 5(a) shows a typical droplet size distribution represented by the number frequency against droplet size. Droplet diameters D_{10}, D_{20}, D_{30}, and D_{32} were 71.55, 83.4, 94.25, and 121.1 μm, respectively (also listed in Table II). The volume histogram plot illustrates that the smaller size droplets do not contribute much to the volume. From Eq. [1], it is obvious that the characteristic diameters D_{30} and D_{32} are heavily influenced by the larger droplets. The mean axial velocity for the spray, as shown in Figure 5(c), was about 47.1 m/s with a root mean square (rms) of 8.9 m/s, although the droplet velocity ranged from 20 to 70 m/s.

Phase Doppler interferometry has the ability to provide a time history of the droplet size and velocity measurements.[34] Time-resolved measurement of the droplet velocity is critical in modeling prediction of droplet solidification behavior, because it can impact the heat transfer between the droplets and the surrounding gas phase. Figure 6 gives the results of droplet axial velocity and size with time and the correlation between the axial velocity and size at a single point for a single run. The relatively invariant time-dependent responses of the droplets and velocities, shown in Figures 6(a) and (b), indicated that the droplet axial velocity and size distribution were relatively invariant throughout the atomization run. The correlation between the axial velocity and droplet diameter (Figure 6(c)) indicated that the smaller droplets had a higher axial velocity than the larger droplets at this measurement point.

B. *Line Characteristics of Droplet Size and Velocity*

Phase Doppler interferometry is a spatially resolved single droplet counting technique. As a result, extensive and tedious measurements would be needed if characterization of the entire spray were required. In the current experiment, the luxury of continuous flow is not available, so this problem is further exacerbated. To improve efficiency, line scanning through the spray was used to characterize the droplet size and velocity and to provide more understanding of droplet size and velocity variation trends throughout the metal spray. The relatively invariant time-dependent responses of the droplets and velocities, as discussed in Section A, help support the validity of this application. Figures 7 and 8 show the results obtained from X-direction scanning

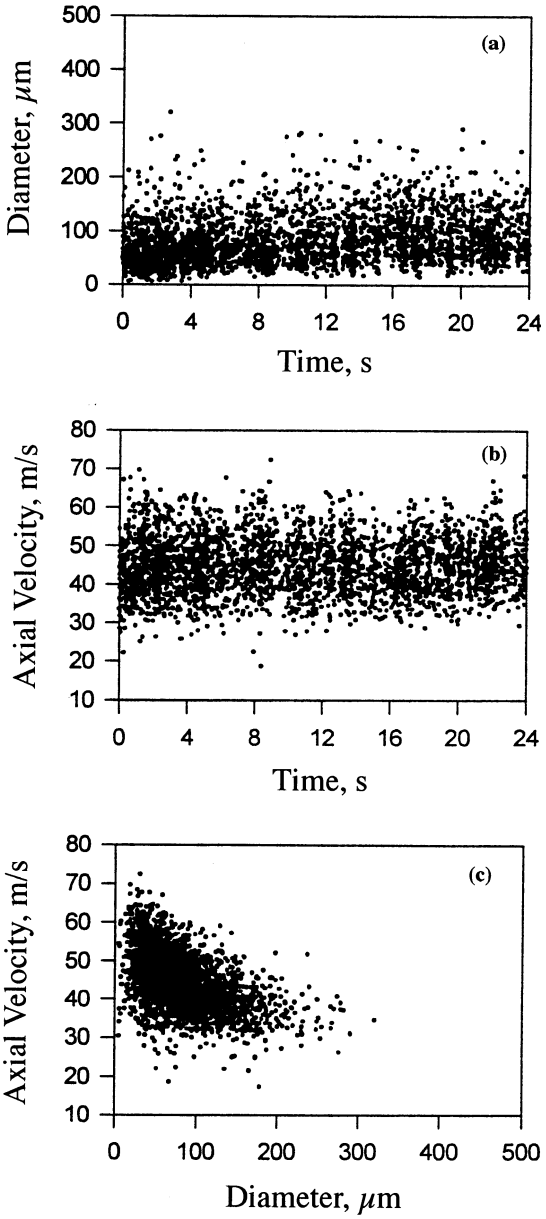

Fig. 6—Function of (*a*) the droplet size and (*b*) the axial velocity with time, and (*c*) correlation between axial velocity and size under the same conditions as in Fig. 5.

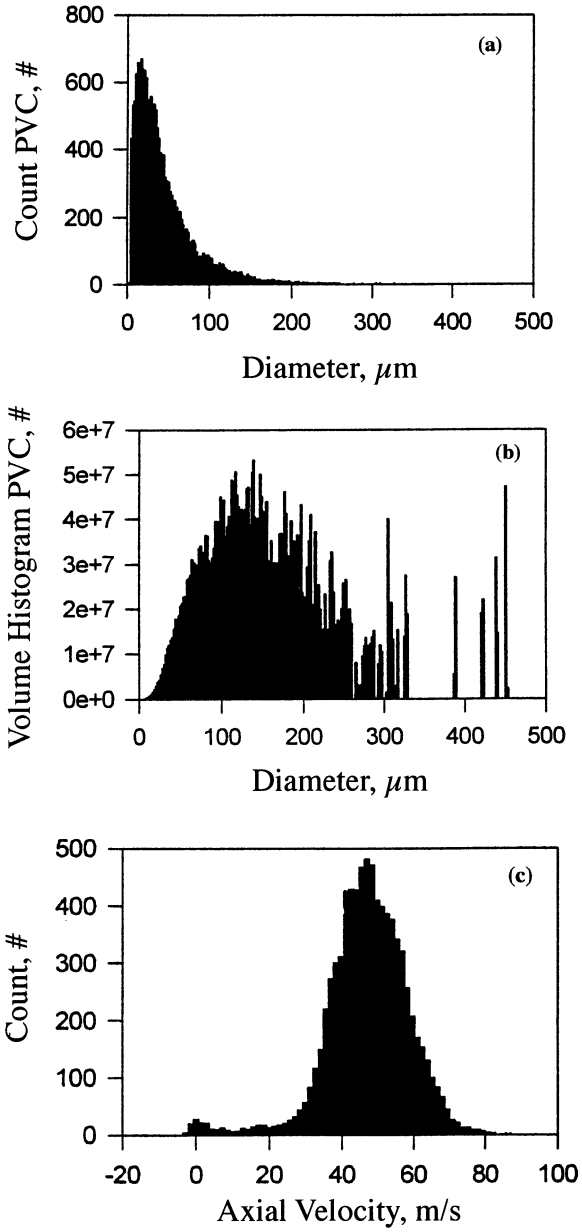

Fig. 7—Measurements along the *X* direction (*Y* = 0 and *Z* = 152.4 mm) for an atomizing gas pressure of 310 kPa (run 19): (*a*) droplet count, (*b*) droplet volume histogram, and (*c*) the axial velocity.

of the spray (along liquid nozzle slit opening, $Y = 0$, and $Z = 152.4$ mm) and *Y*-direction scanning of the spray (perpendicular to liquid nozzle slit opening, $X = 0$, and $Z = 152.4$ mm) for atomizing gas pressure of 310 kPa. In each case, the sample volume was traversed through the spray at 5 mm/s. Figures 7(c) and 8(c) present the axial velocity number frequency distributions along the *X* and *Y* directions. As listed in Table II, the PDI measured mean velocity and corresponding rms for the entire sample were 47.3 and 21.3 m/s in the *X* direction (Figure 7(c)) and 47.3 and 17.6 m/s in the *Y* direction (Figure 8(c)), respectively. Figure 9, however, shows the droplet axial velocity distribution with position along the *X* direction (Figure 9(a)) and along the *Y* direction (Figure 9(b)), indicating a narrower distribution range of velocity in the *X* direction. Since the sampling period at any given location was constant, a broader distribution indicated larger gradients; that is, the axial velocity distribution along the *X* direction was more homogeneous than that in the *Y* direction. In Figure 9(b), it was apparent that the distribution along the *Y* direction was truncated on the left side due to physical limitation of the optical window. Because the spray was geometrically symmetric in both the *X* and *Y* directions, it can be predicted on the basis of the comparison of Figures 9(a) and (b) that the geometrical spread of the metal spray was wider in the *Y* direction than that in *X* direction at the location of $Z = 152.4$ mm. This was attributed to the atomizing gas flow spreading in the *Y* direction due to the linear atomizer slit geometry and the spray atomization direction.

Comparison of the characteristic diameters obtained along the *X* and *Y* directions is shown in Table II. The D_{10} (43.6 μm) in the *X* direction (Figure 7(a)) was larger than

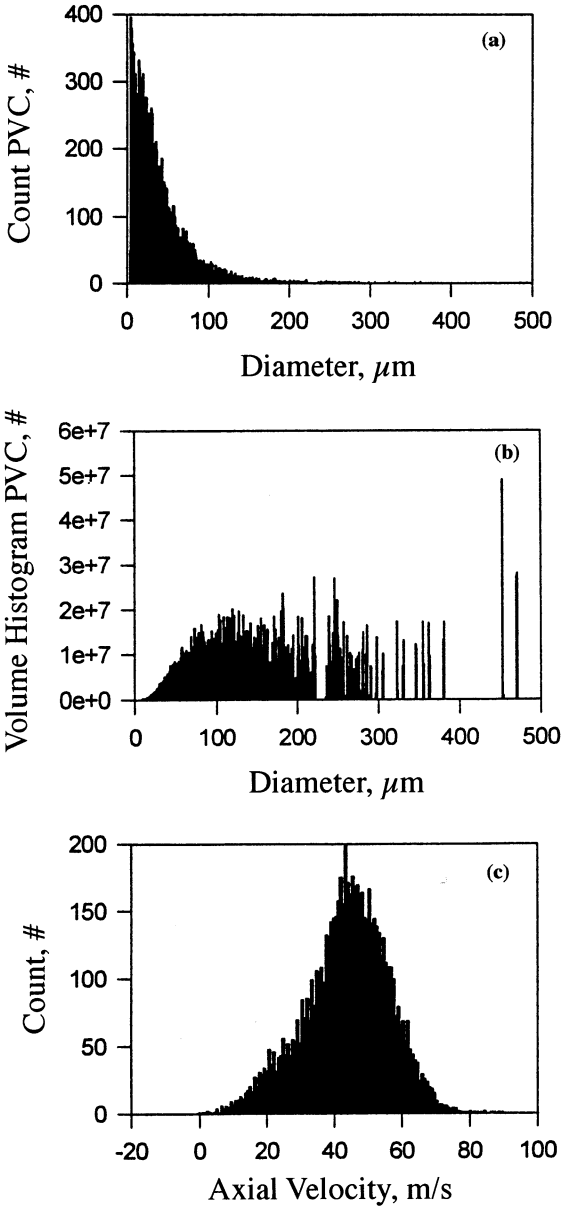

Fig. 8—Measurements along the *Y* direction (*X* = 0 and *Z* = 152.4 mm) for an atomizing gas pressure of 310 kPa (run 20): (*a*) droplet count, (*b*) droplet volume histogram, and (*c*) the axial velocity.

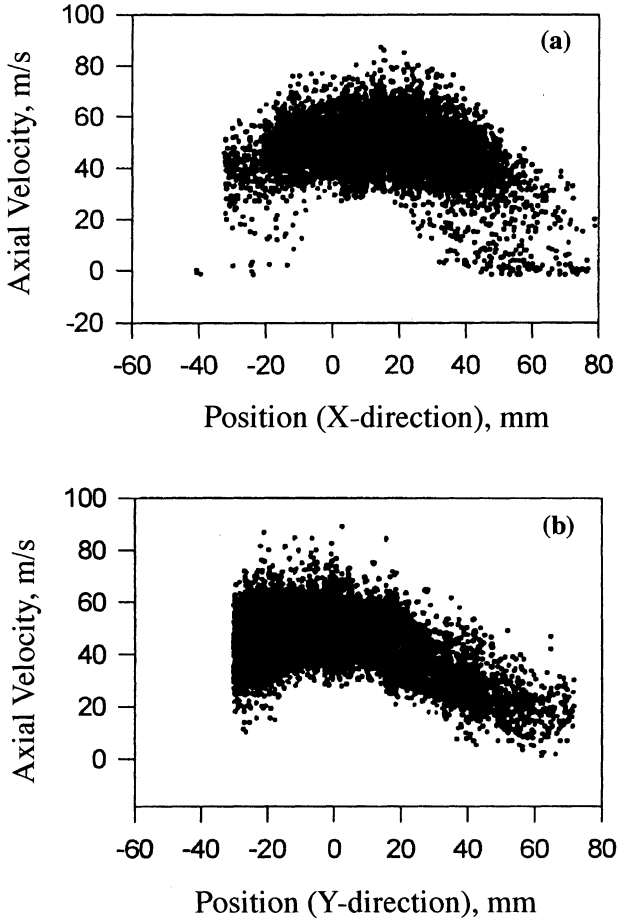

Fig. 9—Comparison of the droplet axial velocity distribution with position at 310 kPa (*a*) along *X* direction (run 19) and (*b*) along *Y* direction (run 20).

the D_{10} (37.17 μm) in the *Y* direction (Figure 8(a)), indicating that the relative fraction of small size powder in the *Y* direction of the spray is higher than that in the *X* direction. The ratio of D_{30} to D_{10}, an indicator of the spread of the size number distribution,[10] showed that the droplet size along the *X* direction (D_{30}/D_{10} = 1.713) exhibited a narrower distribution than that along the *Y* direction (D_{30}/D_{10} = 1.864). This is attributed to the breakup process, which results in a long core of material along the *X* direction, which gives rise to larger droplets. Along the *Y* direction, the greatest shear is available, thus leading to the finest droplets at the edges of the spray. As in Figure 5(b), the volume histogram plots in Figures 7(b) and 8(b) revealed isolated events in the diameter size contributing a significant amount of volume to the sample. After extensive evaluation, it was concluded that the isolated events appeared to be actual droplets. This illustrates a need to carefully assess the statistics of the process to ensure that adequate samples are obtained. With more sampling time, the likelihood of observing these infrequent droplets increased. This must be considered in the current applications since the run duration was inherently short. Figure 10 shows the correlation between the axial velocity and the size of droplets in both scanning directions. The results indicate that the axial velocity for the larger droplet size range, for example, for the droplets with sizes larger than 100 μm, in the *Y* direction exhibited a broader distribution than that in the *X* direction. Note also the bimodal nature along the *X* direction (Figure 10(a)). This was attributed to the global motion of the gas inside the spray chamber, which tended to recirculate metal powders.

Characteristics of PDI point and line scanning measurements can be summarized with a comparison of characteristic diameters and mean velocities. This was carried out for run 13 (*X* = 20 mm, *Y* = 0, and *Z* = 152.4 mm) and run 19 (along *X* direction, *Y* = 0, and *Z* = 152.4 mm) at a pressure of 310 kPa. Based on Table II, droplet size and velocity distribution for both point (run 13) and line (run 19) can be compared. The SMD and mean axial velocity were similar for both conditions. The mean velocity, for example, was 47.1 m/s (run 13) and 47.3 m/s (run 19), respectively. Other parameters, such as D_{10}, D_{20}, D_{30}, and the rms of the axial velocity, however, were significantly different. The axial velocity rms, for example, was 8.9 and

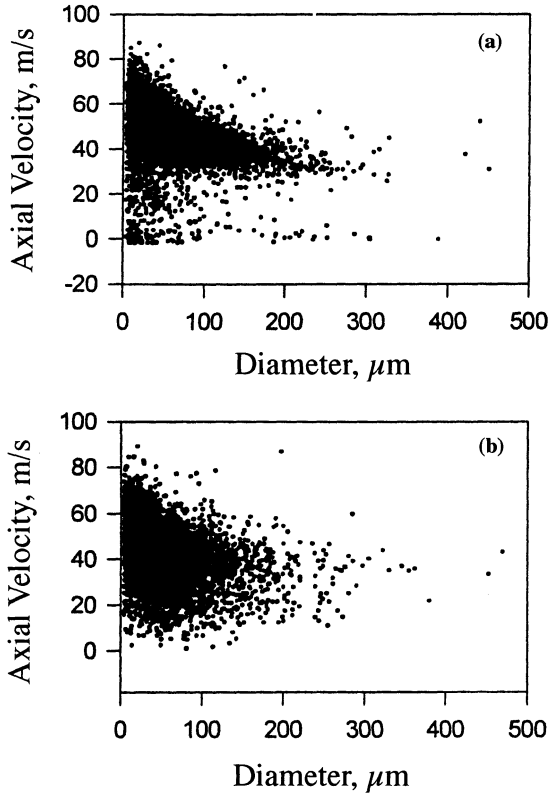

Fig. 10—Comparison of correlation between axial velocity and size obtained along (*a*) *X* direction (run 19) and (*b*) *Y* direction (run 20).

21.3 m/s for runs 13 and 19, respectively. Note also that the numerical mean diameter D_{10} was 71.55 μm (run 13) and 43.6 μm (run 19). The ratio of D_{30} to D_{10} indicated that line measurement (D_{30}/D_{10} = 1.713) exhibited a broader distribution of droplet velocity and size than point measurement (D_{30}/D_{10} = 1.32). This is not surprising and illustrates that the particle size distribution varies throughout the spray. This must be accounted for in a proper model or optimization process.

C. *Influence of Atomization Pressure on Droplet Size and Velocity*

Results of powder droplet size, volume histogram, and axial velocity distributions and correlations between axial velocity and size along the *X* direction for different atomizing gas pressures of 310, 345, and 379 kPa are summarized and compared in this section. Note that the data at 379 kPa were obtained over the range of $X = -40$ to $+65$ mm rather than -40 to $+80$ mm.

1. *Droplet size and distribution*

Figure 11 shows the numerical mean diameter (D_{10}), volume mean diameter (D_{30}), and SMD (D_{32}) obtained at atomizing gas pressures of 310, 345, and 379 kPa (also listed in Table II). The D_{10}, D_{30}, and D_{32} decrease with increasing atomizing gas pressure. Figure 12 shows the number frequency distribution of powder sizes for three atomizing gas pressures. The standard deviation for the number distribution can be calculated to characterize the spread of droplet sizes using the following equation:[10]

$$\sigma_n^2 = D_{20}^2 - D_{10}^2 \qquad [2]$$

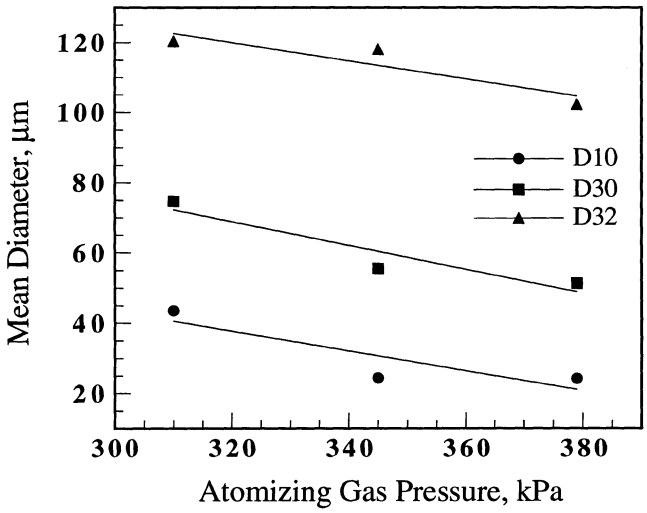

Fig. 11—Mean diameter variation with atomizing gas pressure.

where σ_n is the standard deviation for the number distribution. The terms D_{20} and D_{10} are the surface mean diameter and numerical mean diameter, respectively (listed in Table II). The standard deviations at atomizing gas pressures of 310, 345, and 379 kPa, calculated using Eq. [2], were 39.3, 29.25, and 26.99 μm, respectively. This shows that not only does the average size reduce with increasing gas pressure but so does the width of the size distribution. Figure 13, the droplet size distribution with position for different gas pressures, can provide a direct comparison that the width of the size distribution reduced with increasing gas pressure. As gas pressure increases, the relative fraction of the smaller size range of droplets in the spray increases (Figure 12). Further comparison of the droplet size distribution between Figures 12(a) and (b) indicated that the maximum droplet diameter was decreased at high atomizing gas pressure.

Figure 14 presents the volume histogram distribution at three atomizing gas pressures. It is apparent that the position of the peak of the volume histogram plot shifts to smaller values as the atomizing gas pressure increases.

2. *Droplet velocity and distribution*

Figure 15 presents the results of the axial velocity, which showed that the bimodal axial velocity behavior increased with increasing atomizing gas pressure. A small peak in axial velocity formed around zero. This was attributed to the larger gas momentum for the higher gas pressure cases, which resulted in more pronounced large scale motion within the spray chamber and in turn allowed droplets to be recirculated more easily. This phenomenon was verified by video recordings, which revealed more severe droplet recirculation at higher atomizing gas pressures. In Figure 15, it can also be seen that the position of the large peak of the mean axial velocity was shifted toward the right, indicating that the mean droplet velocity increased with increasing atomizing gas pressure. The peak velocity increased from about 45 to 55 m/s as the atomizing gas pressure increased from 310 to 379 kPa. Figure 15 also indicated that the atomizing gas pressure had little influence on the shape of the primary distribution of axial velocity. To further understand the influence of atomizing gas pressure on the droplet axial velocity and distribution, a com-

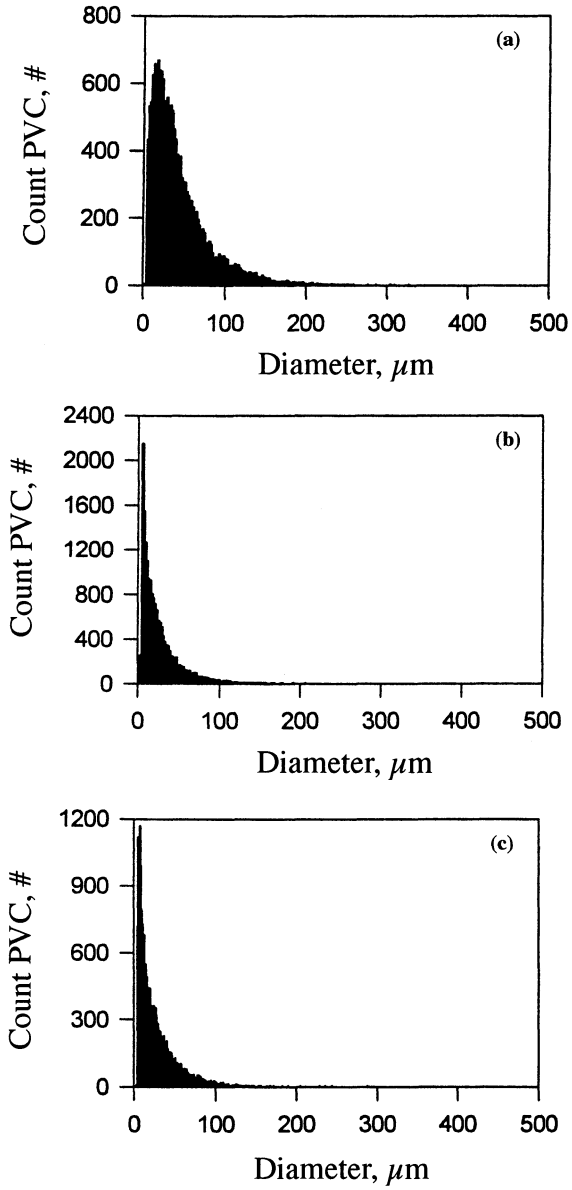

Fig. 12—Comparison of droplet size distribution at different atomizing gas pressures: (*a*) 310 kPa (run 19), (*b*) 345 kPa (run 18), and (*c*) 379 kPa (run 17).

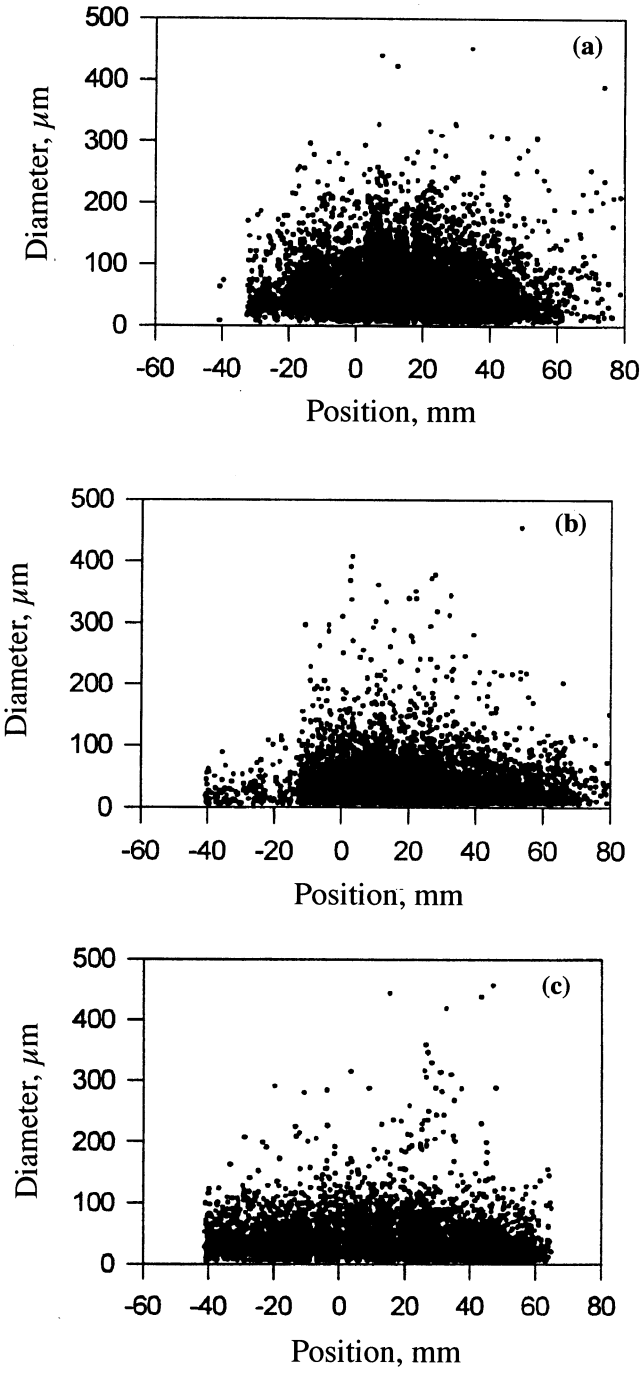

Fig. 13—Comparison of the droplet size distribution with position for (*a*) 310 kPa (run 19), (*b*) 345 kPa (run 18), and (*c*) 379 kPa (run 17).

parison of mean axial velocity and corresponding rms was carried out, as shown in Figure 16. The results show that the mean axial velocity increased as the atomizing gas pressure was increased. The rms, however, remained almost consistent, suggesting little change in the spread of the axial velocity distribution.

D. *Postrun Analysis of Spray Droplet Size Distribution Using Sieving and Diffraction*

The droplet size distribution in the atomization process has been extensively investigated. The spread of the droplet size determines the yields of powders within a specified size range.[35] It has been documented that atomized powders can exhibit monomodal, such as log-normal or normal distribution,[35,36,37] bimodal,[9] and multimodal[38,39] size distributions. In general, however, metal powders produced by gas atomization obey log-normal distribution statistics.[35,36,37]

1. *Powder size distribution by sieving method*

Figure 17 shows the cumulative undersize distributions of powders produced at various atomizing gas pressures. The results demonstrated that the curve shifted toward the finer size value as the atomizing gas pressure increased, which indicated that the powder size was refined with increasing atomizing gas pressure. The mass median diameter (d_{50}), determined from Figure 17 and listed in Table III, showed that the mass median diameter decreased as atomizing gas pressure increased. Figure 18 presents the cor-

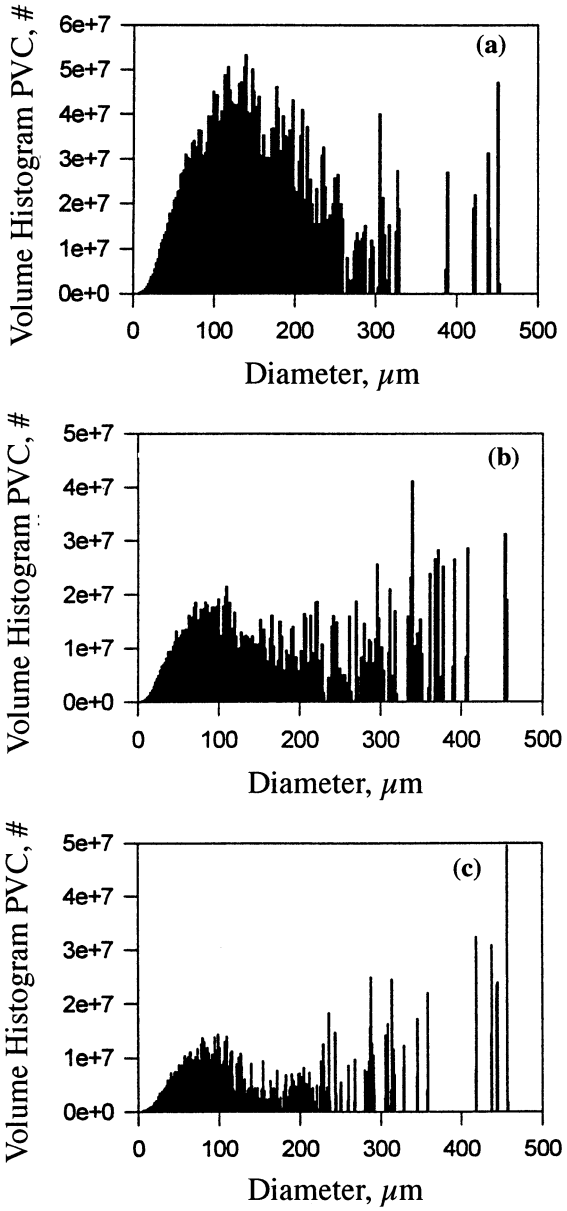

Fig. 14—Comparison of volume histogram distribution at different atomizing gas pressures: (*a*) 310 kPa (run 19), (*b*) 345 kPa (run 89), and (*c*) 379 kPa (run 17).

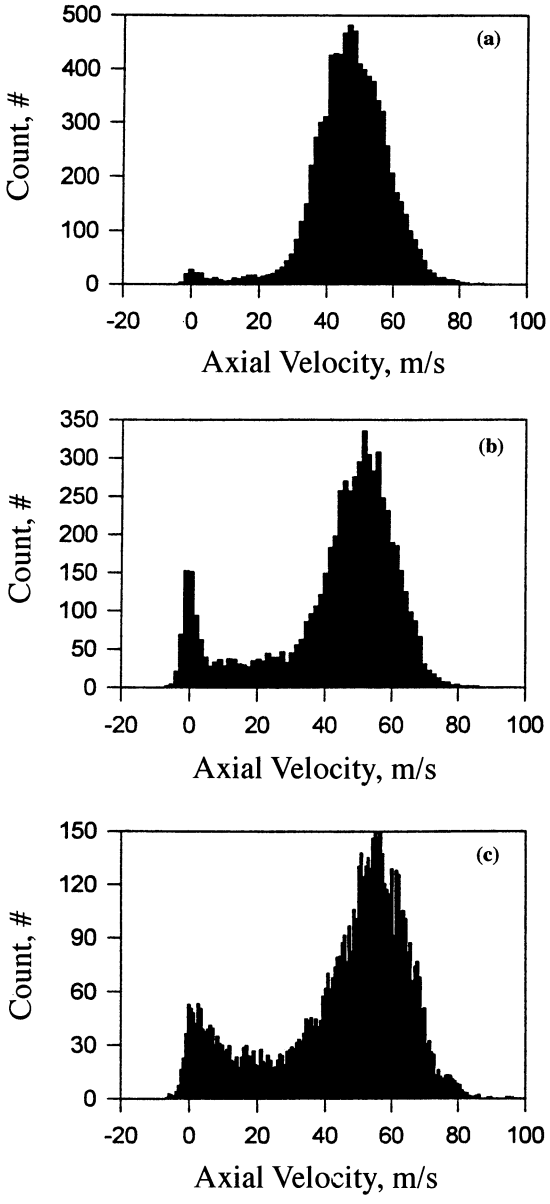

Fig. 15—Comparison of axial velocity distribution at different atomizing gas pressures: (*a*) 310 kPa (run 19), (*b*) 345 kPa (run 89), and (*c*) 379 kPa (run 17).

relation of powder weight percentage with powder size range. In Figure 18, it can be seen that the percentage of the smaller powder size range increased with increasing atomizing pressure, whereas for the larger powder size range, the weight percentage was higher for lower atomizing gas pressure. The sieving distribution of powder sizes indicated that bimodal or multimodal distribution of powder size occurred on the basis of the weight percentage with powder size. Because the size of the sieving screens is not equally discretized, the frequency distribution of the powder weight percentage obtained by the mechanical sieving method may not accurately represent the actual continuous distribution of the number frequency of powder weight percentage against powder diameter. Another form of representation of the cumulative number with powder size, as shown in Figure 19 for atomizing gas pressure of 310 kPa, showed a straight line behavior. This was consistent with previous

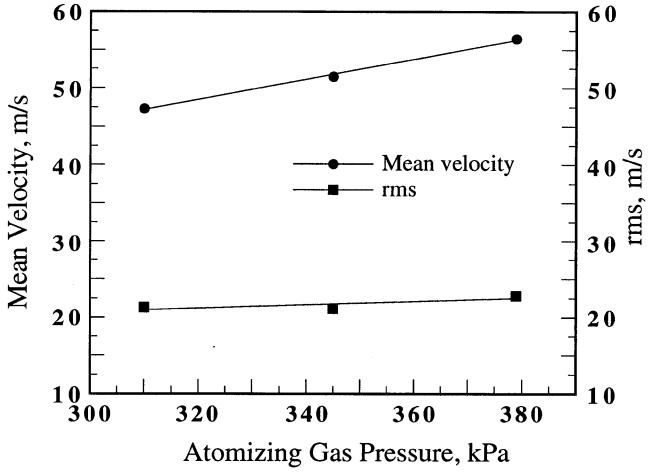

Fig. 16—Mean velocity and rms variation with atomizing gas pressure.

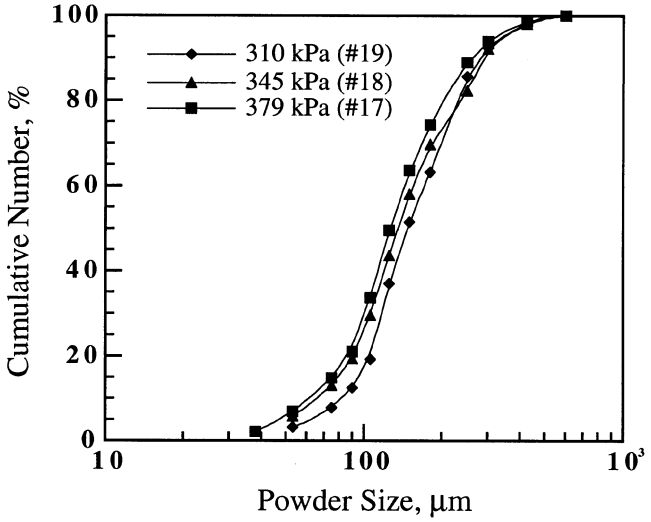

Fig. 17—Comparison of the weight cumulative undersize at different atomizing gas pressures for aluminum alloy.

Table III. Sieving and PDI Results for SMD at Different Atomizing Pressures

Size Range (μm)	Average Diameter (μm), $\bar{x}$	Weight Percentage 379 kPa (17)	345 kPa (18)	310 kPa (19)
0 to 38	19	2.17	—	—
38 to 53	45.5	4.63	—	—
(0 to 53)	26.5	—	5.83	3.17
53 to 75	64	8.13	7.25	4.63
75 to 90	82.5	6.12	6.27	4.57
90 to 106	98	12.64	10.27	6.88
106 to 125	115.5	15.87	14.07	17.69
125 to 150	137.5	14.08	14.44	14.65
150 to 180	165	10.56	11.57	11.67
180 to 250	215	14.79	16.61	22.32
250 to 300	275	4.97	5.92	6.92
300 to 425	362.5	4.75	5.82	5.77
425 to 600	512.5	1.29	1.98	1.76
d_{50}		126.6	135.5	147.9
$\Sigma(d\phi/x)$		0.9524	0.8537	0.796
SMD (d_{32})		105.0	117.1	125.6
SMD (PDI)		102.4	118.2	120.4

results suggesting that the powder size exhibited a log-normal distribution.[10,36,40]

2. *Powder size distribution by laser diffraction*

Alternatively, another optical technique, laser diffraction, can be applied to the collected sample. Laser diffraction is a technique that measures a group of droplets as a whole distribution, and so it is also referred to as ensemble laser diffraction.[41,42,43] In laser diffraction technique, the diffraction component of scattered light, generated as the droplets move across the laser beam, is collected to determine the size of a droplet.[41,42,43] Among the three forms of the scattered light (diffracted light, reflected light, and refracted light), diffracted light exhibits the least sensitivity to droplet shape and optical properties. For characterization of the droplet size and distribution in the entire spray, a commercial unit *Insitec* Ensemble Particle Concentration and Size (EPCS) system was used in the present study. Figure 20 shows the off-line laser diffraction measurement of the powders produced in run 17 at 379 kPa. The cumulative volume and volume frequency of the droplets were presented, indicating a monomodal distribution. A laser diffraction instrument measures the diameters relating to the volume of droplets such as $Dv(10)$, $Dv(50)$, $Dv(90)$, and D_{32}. For example, volume median diameter $Dv(50)$ is a diameter at which 50 pct of the total droplet volume is in droplets of smaller diameter.[33] Figure 21 gives the laser diffraction results of the preceding diameters for runs 17 through 19 at the gas pressure of 310, 345, and 379 kPa, respectively. It can be seen in the figure that the diameters of $Dv(10)$, $Dv(50)$, $Dv(90)$, and D_{32} decrease with increasing gas pressure, consistent with the PDI and sieving results.

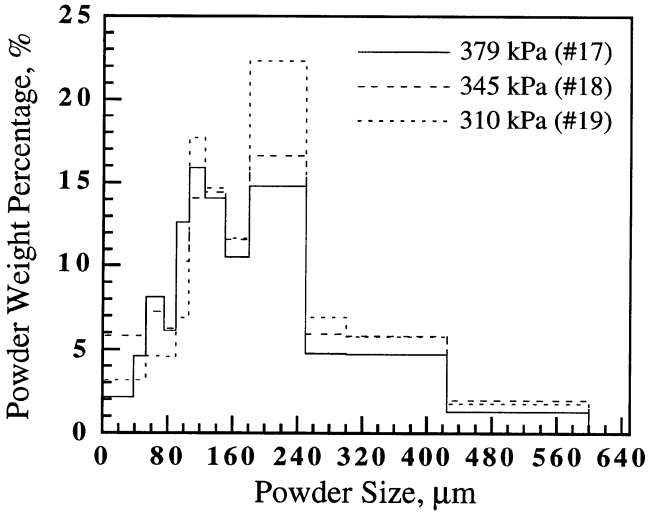

Fig. 18—Comparison of the variations of powder weight percentages with different powder size ranges at different atomizing pressures for 3003 aluminum alloy.

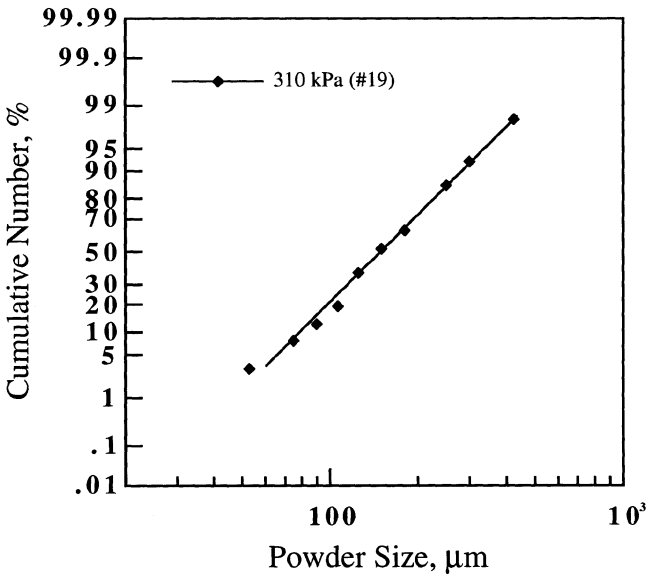

Fig. 19—Cumulative number with powder size for atomizing gas pressure of 310 kPa (run 19), which shows a straight line behavior, suggesting that powder size exhibits a log-normal distribution.

E. *Comparison of SMD*

The Sauter mean diameters obtained, *in situ*, by PDI and postrun laser diffraction and sieving can be compared. The

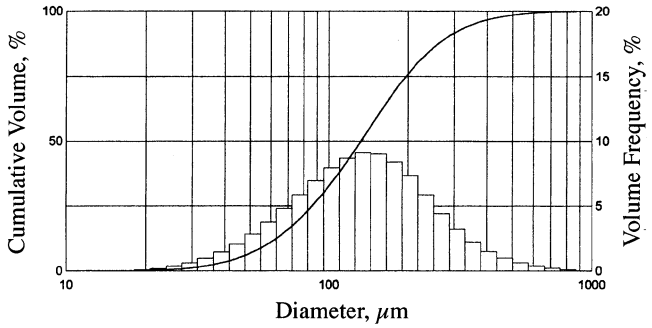

Fig. 20—Size distribution of aluminum powders (run 17) for atomizing gas pressure of 379 kPa using light diffraction (*Insitec* EPCS).

sieving results of powders obtained at different atomizing pressures are presented in Table III. In order to characterize the entire spray, the Sauter mean diameter was calculated, on the basis of the sieving results, using the following equation:[36]

$$d_{32}\ (\text{SMD}) = \frac{\Sigma \bar{x}^3\ dN}{\Sigma \bar{x}^2 dN} = \frac{\Sigma d\phi}{\Sigma\left(\frac{\bar{x}^3\ dN}{\bar{x}}\right)} = \frac{100}{\Sigma\ (d\phi/\bar{x})}, \quad [3]$$

where $d\phi$ is the content (weight percentage) of powders in the size range, and $\bar{x}$ is the average diameter of powders in the size range. The calculated results using Eq. [3] are also summarized in Table III. The SMDs from laser diffraction and sieving methods were compared in Figure 22, indicating a consistent variation with gas pressure. The difference between the SMDs obtained by diffraction and sieving may be attributed to the influence of droplet shape on the measurement results.[44] Sieving measures the narrowest droplet cross-sectional area as droplets randomly pass through the square mesh opening. Laser diffraction, however, allows a statistical sampling of all possible orientations of the droplets as they pass through the laser beam in a turbulent flow. This method, therefore, statistically randomizes the effect of droplet shape on the size distribution.[44] Note also that the *Insitec* EPCS diffraction instrument has the ability to measure spherical droplets and irregularly shaped droplets with an aspect ratio up to 2:1.[41]

In Figure 22, the SMDs obtained by PDI are also shown, and it can be seen that the SMDs obtained by PDI, diffraction, and sieving techniques exhibited a reasonable agreement and a consistent variation with gas pressure. Note that the PDI results were obtained, *in situ*, along a single line scanning through the spray (along the liquid nozzle slit), whereas the diffraction and sieving results accounted for the postrun analysis of the entire powder distribution. Due to the basic difference in sampling technique, some differences in SMD should be expected. The PDI results indicated that the finer droplets were present away from the *X*- and *Y*-axes. Therefore, it might be anticipated that the sieving results of SMD should be smaller than the PDI results of SMD, since the sieving would account for all the finer droplets in both the *X*- and *Y*-axes. The results in Table III do not, however, show a significant difference between the PDI and sieving methods. This may be explained by some larger droplets not being accounted for by PDI due to their irregular shapes. Of course, the PDI provides the opportunity for significantly more information about the spray than does the sieving.

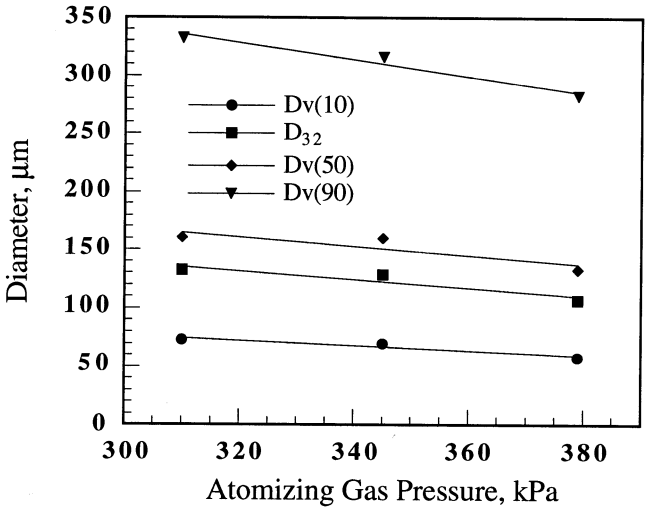

Fig. 21—Diameter variation with atomizing gas pressure obtained using light diffraction (run nos. 17 through 19).

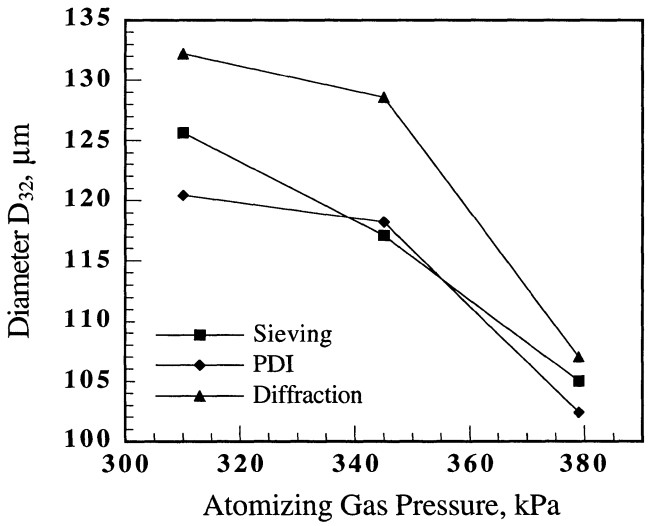

Fig. 22—SMD at different gas pressures obtained using sieving, PDI, and light diffraction, respectively (run 17 through 19).

F. *Measurement Uncertainty*

1. *Spray repeatability*

As discussed in previous sections, it is useful to assume little run-to-run variation in the experiment. In order to understand the repeatability of the experiment, different linear atomization runs at an atomizing gas pressure of 310 kPa were carried out and characterized by droplet size distribution using the mechanical sieving method. Figure 23 gives the results of cumulative percentage undersize distribution of powders obtained by the sieving, indicating that three distribution curves were well matched. Table IV summarizes the variation in mass median diameters (d_{50}) and the calculated SMDs using Eq. [3]. The values of the mass median diameter and SMD for different experimental runs under the same experimental conditions were similar.

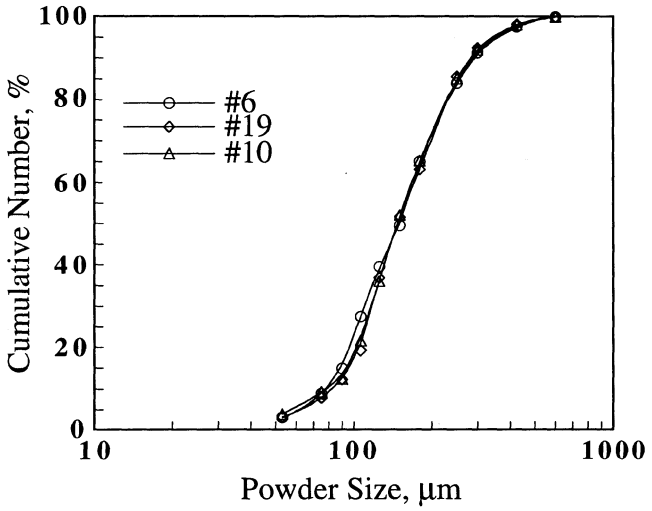

Fig. 23—Sieving results for two runs at atomizing pressure of 310 kPa.

Table IV. Mass Median Diameter and SMD at 310 kPa Atomizing Pressure

Run Number	Mass Median Diameter (d_{50}), μm	Sauter Mean Diameter (d_{32}), μm
6	150.4	122.7
10	147.2	121.5
19	147.9	125.6

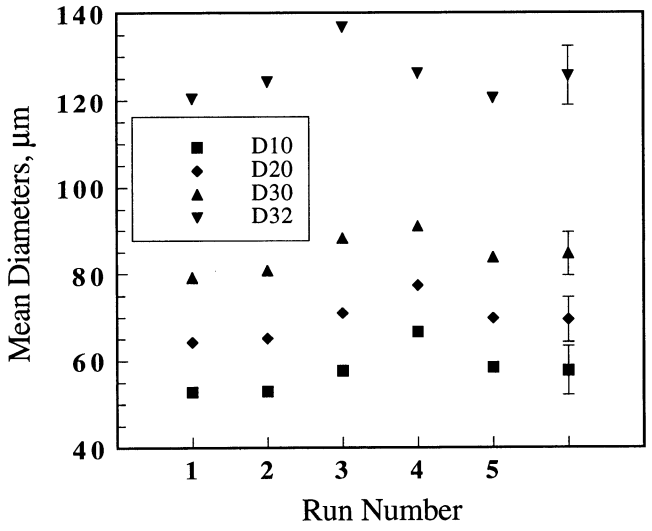

Fig. 24—Characteristic diameters and corresponding averaged values with standard deviations for different experimental runs at a gas pressure of 276 kPa (X = 15 mm, Y = −12.5 mm, and Z = 175 mm).

2. *Phase Doppler Interferometry*

Measurement of the relatively infrequent large droplets and/or variation in average signal-to-noise ratios at the different atomizing pressures can affect the measurement. To resolve this issue, extensive experimental runs should be taken at the same position to determine the uncertainty associated with sampling limitations. Precise determination of the PDI measurement uncertainty, however, is not straightforward. In the current research, experiments were carried out to characterize the uncertainty relating to run-to-run measurements at the same location and same atomizing gas pressure. Figure 24 shows the results of the D_{10}, D_{20}, D_{30}, and D_{32} for five different runs obtained by PDI at atomizing gas pressure of 276 kPa and at a location of X = 15 mm, Y = −12.5 mm, and Z = 175 mm. The mean value of these parameters and standard deviations about the mean are also shown in Figure 24. The results provide a measure of the expected variation in measurement of D_{10}, D_{20}, D_{30}, and D_{32}, from run to run. The SMD D_{32}, for example, has an average value of 125.6 μm with a standard deviation of 6.7 μm for five experimental runs. Figure 25 gives the results of the droplet axial velocity and corresponding rms for the runs presented in Figure 24. The averaged value (67.2 m/s) of the droplet mean axial velocities and statistical standard deviation (3.97 m/s) are also shown in Figure 25. In general, the experimental measurement uncertainty resulting from run-to-run variation was approximately ±5 pct. Possible reasons for the observed variations in the measured mean diameter and velocity include the following: (1) slight variations in gas pressure from experiment to experiment; and (2) slight changes in sampling location, since the metal spray experiment exhibited a certain degree of spatial variation due to reassembly.

Table V. Mean Diameters Obtained by PDI at a Gas Pressure of 276 kPa (corresponds to Fig. 24)

	D_{10}, μm	D_{20}, μm	D_{30}, μm	D_{32}, μm
Run 1	52.8	64.3	79.2	120.4
Run 2	53.0	65.2	80.8	124.3
Run 3	57.7	70.9	88.2	136.8
Run 4	66.6	77.4	91.1	126.2
Run 5	58.5	69.8	83.8	120.5
Mean	57.7	69.5	84.6	125.6
Standard deviation	5.6	5.2	5.0	6.7

IV. SUMMARY AND CONCLUSIONS

For many years, PDI has been successfully used for simultaneous droplet size and velocity measurements in combustion and other environments. This article provides extensive PDI measurements of the droplet size and velocity in metal sprays. Uncertainties associated with the metal spray repeatability and PDI measurements were established at ±5 pct through a series of tests. Key findings are summarized below as follows.

1. The PDI point characteristics of the metal spray demonstrated that the droplet axial velocity and size as a function of time were relatively consistent throughout the experimental run at a given measurement point.
2. The PDI line measurements provided the variation of droplet size and velocity with position (or time), delineating the spatial characteristics of the droplet size and velocity in the metal sprays. The droplet axial velocity showed a bimodal behavior and this became more apparent with increasing atomizing gas pressure, indicating that droplet recirculation became more common at higher atomizing pressures. The peak position of the axial velocity distribution was shifted toward the right, showing that the mean velocity increased with increasing atomizing gas pressure.

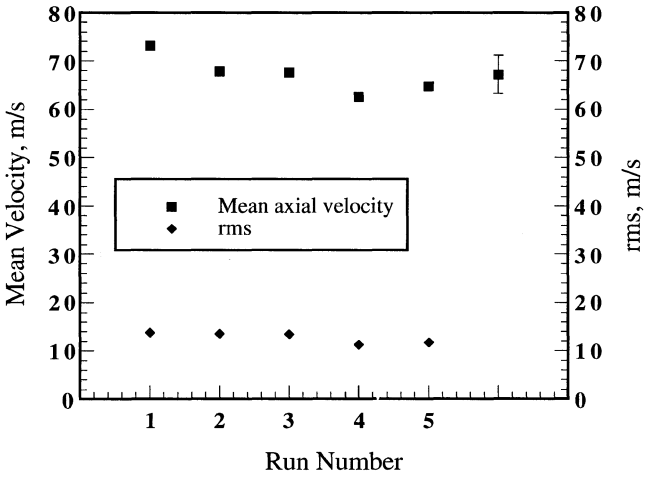

Fig. 25—Mean axial velocity, corresponding rms, and an averaged value with standard deviation bars for different experimental runs at a gas pressure of 276 kPa ($X = 15$ mm, $Y = -12.5$ mm, and $Z = 175$ mm).

3. The characteristic diameters, D_{10}, D_{20}, D_{30}, and D_{32} obtained by PDI, showed that powder droplet size decreases with increasing atomizing gas pressure and exhibits a monomodal distribution. The line characteristics of the droplet size and distribution can also be delineated by using the ratio of D_{30} to D_{10}, an indicator of the spread of the droplet size distribution. Comparison of the ratio of D_{30} to D_{10}, for example, indicated that the spread of the droplet size distribution along the X direction exhibited a narrower distribution than that along the Y direction. This illustrates that the size distribution varies throughout the spray and using ensemble and overall averages may be misleading.
4. Laser diffraction and mechanical sieving methods were used for the postrun analysis of the powder size and distribution. The results indicated a consistent variation with gas pressure. The mass (volume) median diameter and the SMD, for example, decreased with increasing atomizing gas pressure. A difference resulted from diffraction and sieving may be attributed to the influence of the powder shape.

ACKNOWLEDGMENTS

The authors acknowledge the research funding support (Grant No. DE-FC07-94ID13238) under the United States Department of Energy and the Aluminum Company of America (Alcoa, Pittsburgh, PA). The authors also acknowledge the NSF (Grant No. DMI 9528684) for support. Particular thanks also go to Messrs. Frank Baker and William Straub, Alcoa, for their support and help. The authors also thank Messrs. Irwin Sauer and Weyland Leong, University of California–Irvine, for their contributions to this project. In addition, one of the authors (EJL) acknowledges the Alexander von Humboldt Foundation in Germany for support of his sabbatical visit at the Max-Planck-Institut Fur Metallforschung (Stuttgart, Germany).

REFERENCES

1. E.J. Lavernia, J.D. Ayers, and T.S. Srivatsan: *Int. Mater. Rev.*, 1992, vol. 37, pp. 1-44.
2. P.S. Grant:*Progr. Mater. Sci.*, 1995, vol. 39, pp. 497-545.
3. E.J. Lavernia and Y. Wu: *Spray Atomization and Deposition*, John Wiley & Sons, New York, NY, 1996, pp. 263-381.
4. V.G. McDonell, E.J. Lavernia, and G.S. Samuelsen: in *Synthesis and Analysis in Materials Processing: Advances in Characterization and Diagnostics of Ceramics and Metal Particulate Processing*, E.J. Lavernia, H. Henein, and I. Anderson, eds., TMS, Warrendale, PA, 1989, pp. 13-37.
5. P. Mathur, D. Apelian, and A. Lawley: *Acta Metall.*, 1989, vol. 37, pp. 429-33.
6. S. Annavarapu, D. Apelian, and A. Lawley: *Metall. Trans. A*, 1990, vol. 21A, pp. 3237-56.
7. C.A. Tsao and N.J. Grant: *Int. J. Powder Metall.*, 1994, vol. 30, pp. 323-33.
8. O.P. Pandey and S.N. Ojha: *PMI*, 1991, vol. 23, pp. 291-95.
9. B.P. Bewlay and B. Cantor: *Metall. Trans. B*, 1990, vol. 21B, pp. 899-912.
10. A.D. Yule and J.J. Dunkley: *Atomization of Melts for Powder Production and Spray Deposition*, Clarendon Press, Oxford, United Kingdom, 1994, pp. 247-257 and pp. 309-12.
11. P.D. Prichard and R.P. Dalal: in *Superalloys 1992*, S.D. Antolovich, R.W. Stusrud, R.A. MacKay, D.L. Anton, T. Khan, R.D. Kissinger, and D.L. Klarstrom, eds., TMS, Warrendale, PA, 1992, pp. 205-14.
12. A.G. Leatham and A. Lawley: *Int. J. Powder Metall.*, 1993, vol. 29, pp. 321-29.
13. K. Ogata, E. Lavernia, G. Rai, and N.J. Grant: *Int. J. Rapid Solidification*, 1986, vol. 2, pp. 21-35.
14. P. Mathur, S. Annavarapu, D. Apelian, and A. Lawley: *J. Met.*, 1989, vol. 41 (8), pp. 23-28.
15. A.L. Moran and D.R. White: *JOM*, 1990, vol. 42 (7), pp. 21-24.
16. R.D. Payne, A.L. Moran, and R.C. Cammarata: *Scripta Metall. Mater.*, 1993, vol. 29, pp. 907-12.
17. R.D. Payne, M. Allen Matteson, and A.L. Moran: *Int. J. Powder Metall.*, 1993, vol. 29, pp. 345-51.
18. N.J. Grant: in *Casting of Near Net Shape Products*, Y. Sahai, J.E. Battles, R.R. Carbonara, and C.E. Mobley, eds., TMS-AIME, Warrendale, PA, 1988, pp. 257-72.
19. F.W. Baker, R.L. Kozarek, and G.J. Hildeman: *Proc. 2nd Int. Conf. on Spray Forming*, J.V. Wood, ed., Woodhead Publishing Limited, 1993, pp. 395-97.
20. V.G. McDonell and G.S. Samuelsen: *Combust. Sci. Technol.*, 1990, vol. 74, pp. 343-59.
21. W.D. Bachalo: *Appl. Opt.*, 1980, vol. 19, pp. 363-70.
22. F.K. Durst and M. Zare: *LDA-Symp. 1975 Accuracy of Flow Measurements by Laser Doppler Methods*, Copenhagen, Denmark, 1975, pp. 14-16
23. M. Saffman, P. Buchhave, and H. Tanger: *Proc. 2nd Int. Symp. on Applications of Laser Anemometry to Fluid Mechanics (Lisbon, Portugal)*, R.J. Adrian, D.F.G. Durão, F. Durst, H. Mishina and J.H. Whitelaw, eds., LADOAN, Portugal, 1984, pp. 85-103.
24. K. Bauckhage, H.-H. Flogel, U. Fritsching, and R. Hiller: *Proc. 2nd Int. Conf. on Laser Anemometry—Advances and Applications (Strathclyde, Scotland)*, J. Turner and S. Fraser, eds., Springer-Verlag, 1987, pp. 347-54.
25. J. Domnick, J. Raimann, G. Wolf, A. Berlemont, and M.-S. Cabot: *Proc. 7th Int. Conf. on Liquid Atomization and Spray System*, Seoul, Korea, 1997, vol. II, pp. 999-1006.
26. P.P. Maher, P.S. Grant, B. Cantor, and L. Katgerman: *Proc. 1st Int. Conf. on Spray Forming*, Swansea, UK, 1990, Section 3, Paper 15.
27. B.P. Bewlay and B. Cantor: *Mater. Sci. Eng.*, 1989, vol. A118, pp. 207-22.
28. P.S. Grant, P.P. Maher, and B. Cantor: *Mater. Sci. Eng.*, 1994, vols. A179–180, pp. 72-76.
29. T. Wriedt, K.A. Bauckhage, and A. Shone: *IEEE Trans. Instrum. Meas.*, 1989, vol. 38, pp. 984-90.
30. K.M. Ibrahaim and W.D. Bachalo: *Proc. 6th Int. Symp. on Applications of Laser Techniques to Fluid Mechanics*, Lisbon, Portugal, July 20-23, 1992, paper no. 21.5.
31. Y. Zhou, S.W. Lee, V.G. McDonell, G.S. Samuelsen, R.L. Kozarek, and E.J. Lavernia: *Proc. ILASS-96 (Extended Abstract)*, San Francisco, CA, May 19–22, 1996.
32. Y. Zhou, S.W. Lee, V.G. McDonell, G.S. Samuelsen, R.L. Kozarek, and E.J. Lavernia: *At. Sprays*, 1997, vol. 7, pp. 339-58.
33. *Annual Book of ASTM Standards*, Designation E799-92, ASTM, Philadelphia, PA, 1993, vol. 14.02, pp. 444-48.

34. W.D. Bachalo: *Int. J. Multiphase Flow*, 1994, vol. 20, suppl., pp. 261-95.
35. E.J. Lavernia, T.S. Srivatsan, and R.H. Rangel: *At. Sprays*, 1992, vol. 2, pp. 253-74.
36. A. Ünal: *Mater. Sci. Technol.*, 1987, vol. 3, pp. 1029-39.
37. A. Ünal: *Mater. Sci. Technol.*, 1989, vol. 5, pp. 1027-33.
38. A.J. Aller and A. Losada: *PMI*, 1989, vol. 21 (5), pp. 15-19.
39. F.S. Biancaniello, J.J. Conway, P.I. Espina, G.E. Mattingly, and S.D. Ridder: *Mater. Sci. Eng.*, 1990, vol. A124, pp. 9-14.
40. H. Lubanska: *J. Met.*, 1970, No. 2, pp. 45-49.
41. T.L. Harvill, J.H. Hoog, and D.J. Holve: *Part. Part. Syst. Charact.*, 1995, vol. 12, pp. 309-13.
42. R.A. Robbins, L. Crocco, and I. Glassman: *AIAA J.*, 1963, vol. 1, pp. 1882-86.
43. P.G. Felton: in *Liquid Particle Size Measurement Techniques: 2nd Volume*, ASTM STP 1083, E.D. Hirleman, W.D. Bachalo, and P.G. Felton, eds., ASTM, Philadelphia, PA, 1990, pp. 47-59.
44. D.J. Holve: *Powder Bulk Eng.*, 1994 Feb., pp. 43-49.